Sensors & Actuators: B. Chemical 354 (2022) 131218

Contents lists available at ScienceDirect

Sensors and Actuators: B. Chemical

journal homepage: www.elsevier.com/locate/snb

Vibrating an air bubble to enhance mass transfer for an ultra-sensitive electrochemical sensor

Tianyi Zhang, Peng Zhou, Terrence Simon, Tianhong Cui *

Department of Mechanical Engineering, University of Minnesota, 111 Church Street SE, Minneapolis, MN 55455, USA

ARTICLE INFO

Keywords:
Vibrating air bubble
Streaming flow
Mass transfer
Electrochemical sensor
Anodic stripping voltammetry

ABSTRACT

Rapid mass transfer of analytes is essential for effective electrochemical sensing. Here, we present a vibrating air bubble as a stirrer and evaluate the optimal working frequency. A vibration system that contains a flexible piezoelectric plate coupled with a trapped bubble integrated with a gold working electrode is employed. The vibrational properties and mass transfer of the coupled system are experimentally tested with optical and electrochemical methods, respectively. Streaming flows generated by the vibrating bubble are characterized by visualization to explain the enhancement of mass transport to the working electrode. Compared with a static case, measurements with a vibrating bubble demonstrate a twelve-times enhancement in mass transfer coefficient. Enhanced sensing performance is experimentally quantified with the bubble stirrer and its integrated electrochemical metal ion sensor. This integrated system can be used for various types of electrochemical sensing applications that are limited by slow molecular diffusion.

1. Introduction

Electrochemical methods have drawn considerable attention in chemical and biological detection due to their significant advantages, such as low cost and high sensitivity [1,2]. Normally, for sensing, analytes in the solution, such as metal ions, nucleic acids, and proteins, must accumulate on the surface of the working electrode [3–5]. This requires mass transfer, which includes diffusion, convection, and migration [6]. In static solutions, this process is usually limited by a slow molecular diffusion rate that may take hours for sensing [7], causing a major obstacle to the sensing performance. To overcome this problem, methods involving convective mass transport can be employed. By generating fluid motion near the working electrode, the diffusion layer thickness can be reduced and the molecular transmission rate through the diffusion layer to the reaction interface can be aided by convection [8].

Among various methods of generating liquid flow, streaming flows induced by a vibrating air bubble in the liquid are of increasing interest in recent years [9,10]. The streaming flow of interest in the present paper is due to nonlinear second-order effects in the fluid mechanics that are induced by unsteady surface deformations of a vibrating air bubble [11]. In contrast to a mechanical stirrer, this strategy does not need a movable mechanical component near the sensor, which makes the vibrating bubble a low-cost, low-power, easy-to-integrate method for production of circulating flow. Bubble induced streaming flow has already been utilized in multiple microfluidic applications, such as micropumps [12], chemical switches [13], micromixers [14], microswimmers [15], and acoustic manipulation of organic cells or particles [16]. Detailed classification and introduction of the applications employing streaming flows are summarized in several review papers [17–19].

In the above-mentioned works, vibrating air bubbles are trapped in a rigid structure. Acoustic waves are generated by a piezoelectric transducer attached to the substrate. The waves propagate within the structure to vibrate the bubbles. The optimized working frequencies for bubbles to produce streaming flows, normally considered to be resonance frequencies of the bubble, are usually determined by experiments conducted while documenting with particle image velocimetry (PIV) measurements [20,21]. Such PIV measurement is complicated and time-consuming. Moreover, it has a poor frequency resolution and cannot be used to track the resonance frequency of the bubble in real-time. However, the resonance frequency of a bubble can be directly measured with a laser Doppler vibrometer using a laser spot focused directly on the surface of the bubble [22–24]. The accuracies of both amplitude and frequency using this method can be extremely high. But such measurements can be influenced by the liquid itself, and the

* Corresponding author.
E-mail addresses: zhan6202@umn.edu (T. Zhang), zhou1161@umn.edu (P. Zhou), simon002@umn.edu (T. Simon), cuixx006@umn.edu (T. Cui).

https://doi.org/10.1016/j.snb.2021.131218
Received 21 September 2021; Received in revised form 29 November 2021; Accepted 5 December 2021
Available online 9 December 2021

container sidewalls, which limit their applicability. Also used are flexible piezoelectric energy harvesters that detect the vibrational amplitude of a bubble [25] by converting the vibration of the bubble to a voltage signal through a piezo-electric pickup.

Here we propose a stirring strategy for electrochemical measurement, where a piezoelectric-actuated vibrational air bubble stirrer is integrated with a working electrode. A novel method, aiming to detect the resonance frequency and optimal working frequencies of the vibrating air bubble, is demonstrated based on mechanical vibration coupling between the bubble and a flexible plate. In this work, the vibrating system includes a flexible piezoelectric plate coupled to a trapped air bubble, in which the vibrational energy is transferred from the plate to the bubble. The vibrational properties of the coupled system are experimentally investigated with a laser Doppler vibrometer, and the resonance frequency and optimal working frequencies of the bubble are directly related to the frequency response of the piezoelectric plate. Streaming flows induced by the vibrating bubble are characterized by dye tracing under different working frequencies. These flows can be utilized to accelerate mass transport of analytes from the bulk solution toward the sensing electrode surface. With an integrated working electrode and the electrochemical method, we measured the mass transfer coefficient under the influence of the streaming flows. Finally, the performance of the air bubble stirrer with the integrated electrode is evaluated as an electrochemical metal ion sensor.

2. Material and methods

2.1. Reagents

Reagents are potassium ferricyanide (III), potassium chloride, bismuth standard solutions (1000 mg/L in 5% HNO_3), and methylene blue, all purchased from Sigma-Aldrich (St. Louis, MO, United States), and Hydrochloric acid (1.0 N) and sulfuric acid (98%), purchased from Fisher Scientific (Hampton, NH, United States). All solutions are prepared with deionized water from AmeriWater silex deionization system (Dayton, OH, United States).

2.2. Fabrication of bubble actuator and working electrode

A piezoelectric vibrating bubble actuator attached with a working electrode for electrochemical measurements was designed and fabricated in this study. The exploded 3D view and the cross-section of the integrated device are shown in Fig. 1(a) and (b), respectively. The fabrication process consists of four components: A piezoelectric plate (15 mm and 10 mm in diameter for the metal plate and piezoelectric ceramic) are attached to a pre-cut polymethyl methacrylate (PMMA) frame. A circular hole (10 mm in diameter) is cut by a laser cutter. A polyimide (PI) film (25 μm thick) is bonded to the bottom layer of the piezoelectric plate (the metal side), followed by attachment of a polytetrafluoroethylene (PTFE) ring onto the PI surface, located at the center of the plate. The PTFE ring acts as the bubble trapper having inner and outer diameters of 1.7 mm and 2.3 mm. A PMMA thin film (300 μm thick) is cut with a laser to form the contour of the electrode substrate, then is cleaned with ethanol and deionized water. The central hole (4 mm in diameter) is used to accommodate the PTFE ring. The PMMA film is covered by a polyester (PE) shadow mask also fabricated with the laser cutter. Subsequently, a gold layer (100 nm thick) is sputtered onto the PMMA film to form the working electrode. Finally, the working electrode is attached to the PMMA frame. The gap between the PI film and the working electrode substrate is 500 μm. The working electrode and the piezo plate are connected to wires with silver adhesive. A photo of the fabricated device is shown in Fig. S1 of the supplemental material.

2.3. Characterization of vibration and streaming flow

The experimental setup is shown in Fig. 1(b). A laser Doppler

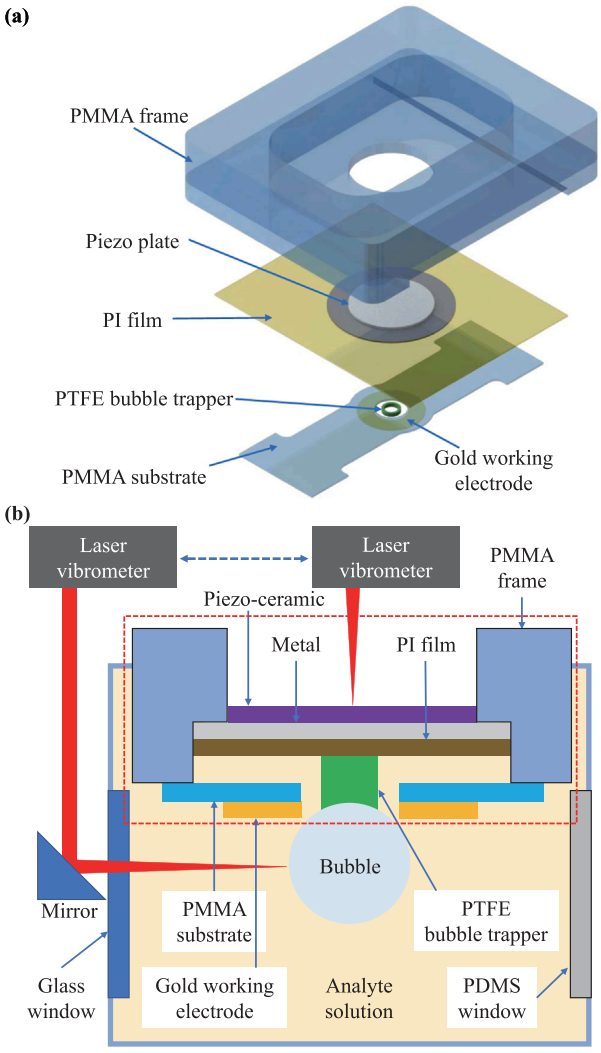

Fig. 1. (a) Exploded 3D view of the vibrating bubble actuator with an attached gold working electrode. (b) Cross-sectional schematic of the device (shown in the red dashed box) and a schematic of the experimental setup.

vibrometer (PSV-400 Polytec Inc., Irvine, CA, United States) is used to characterize the vibrational properties of the piezoelectric plate and the trapped air bubble. The driving alternating voltage is applied by a built-in function generator and is amplified by a linear piezoelectric amplifier (VF-500, Dynamic Structures and Materials, Franklin, TN, United States) before driving the piezoelectric ceramic. The integrated device is placed horizontally in a self-made PMMA cuboid container filled with deionized water. There is a glass window on three sidewalls of the container and a polydimethylsiloxane (PDMS) window on the last sidewall. The glass window is for light transmission, while the PDMS window is used to pass the needle through to introduce the bubble gas. A photo of the device with the container is shown in Fig. S1 in the supplemental material. To measure the vibrational properties of the piezo plate, a vertical laser beam from the laser vibrometer is used to scan the upper surface of the piezoelectric ceramic. A 45-degree tilted mirror is employed to steer the laser beam to be horizontal to detect vibration of the air bubble. In the horizontal beam case, the laser beam is carefully focused on the tangent point between the bubble surface and the vertical plane. The movement of the piezo plate in the out-of-plane direction and the amplitude of the bubble are detected successively by the vibrometer.

The air bubble is injected with a needle through the PDMS window and placed on the PTFE bubble trapper. The volume of the bubble is controlled by a microliter pipette connected to the needle. Dye

(10 mmol/L methylene blue) is injected near the bubble by a syringe needle. Optical images of the bubble and dye are captured with a high-speed camera (GS3-U3-23S6M-C, FLIR Systems, Wilsonville, OR, United States) by viewing through the glass window, together with an LED light source located on the opposite side of the container.

2.4. Mass transfer tests and metal ion detection

An electrochemical workstation (PGSTAT302N Metrohm, Riverview, FL, United States) is employed for characterization of the mass transfer coefficient and for metal ion detection, using chronoamperometry and anodic stripping voltammetry (ASV) methods, respectively. A platinum wire (1 mm in diameter) and an Ag/AgCl (in 3.0 mol/L KCl solution) electrode are used as the counter and reference electrodes, respectively. Before the electrochemical measurement is conducted, the gold working electrode is cleaned with the cyclic voltammetry method (from −0.4 V to 1.5 V vs. Ag/AgCl at a scan rate of 0.1 V/s) for 40 scans in a 1 mol/L H_2SO_4 solution.

The chronoamperometry measurement is conducted in a 2 mmol/L $K_3Fe(CN)_6$/0.5 mol/L KCl solution. A conditioning potential of 0.7 V is applied on the gold working electrode for 90 s prior to each measurement. The working potential for mass transfer characterization is − 0.4 V, and the measurement lasts for 90 s, while bubble vibration is maintained. The following four steps are carried out for each of the ASV tests in a 20 ppb Bi^{3+}/0.1 mol/L HCl solution: conditioning the working electrode, background scan, metal deposition and the analytical scan. The conditioning potential is 0.7 V, and the conditioning time is 30 s longer than the deposition time. The square wave voltammetry (SWV) method is used in the two steps of scanning. The SWV parameters are the following: scan window is − 0.3–0.7 V; square wave amplitude and frequency are 25 mV and 25 Hz, respectively; and step potential is 5 mV. In the metal deposition step, the deposition potential is − 0.3 V, and the deposition time is from 30 to 150 s. The bubble vibration is maintained during only the deposition step.

3. Results and discussion

3.1. Characterization of vibrating bubble system and streaming flow

The vibrational properties of the piezo plate and the air bubble are characterized by measuring their frequency responses with the laser Doppler vibrometer. The gold working electrode is removed in this experiment and the following dye tracing experiment to ensure good vision of the bubbles and flow. The piezoelectric ceramic is driven by a frequency chirp signal (from 0.1 to 6 kHz) with an ultra-small voltage amplitude (0.01 V) to avoid generation of complex surface modes of the bubble [26]. Then the detected signal from the surface vibration of the piezo plate and air bubble is subjected to a fast Fourier transform to obtain the response in frequency space at a specific vibrometer scan location. We also measured the mode shape of the piezo plate by scanning the whole surface of the ceramic part of the plate with the vibrometer. Frequency response curves measured at the center point of the piezo plate, where the bubble trapper is located, are shown in Fig. 2(a). When there is no bubble, a single resonance peak is observed (black curve), corresponding to the (0, 1) mode of the circular piezo plate vibrating in a liquid environment. The mode number of (0, 1) is determined by checking the measured mode shape, as shown in Fig. 2(c). The color scale used in the mode shape figures of Fig. 2(c) represents vibrating velocity distributions. The red parts are anti-nodes where the velocity has its maximum value. After an air bubble is placed onto the bubble trapper, the frequency response measurement is taken again. Now, the frequency response curves indicate that the original single resonance peak of the plate is split into two peaks by a deep valley in the middle, making the frequency response curve of the plate appear as a capital letter M (seen for the other four curves excluding the black curve in Fig. 2(a)). It is found by checking the mode shapes obtained at each of

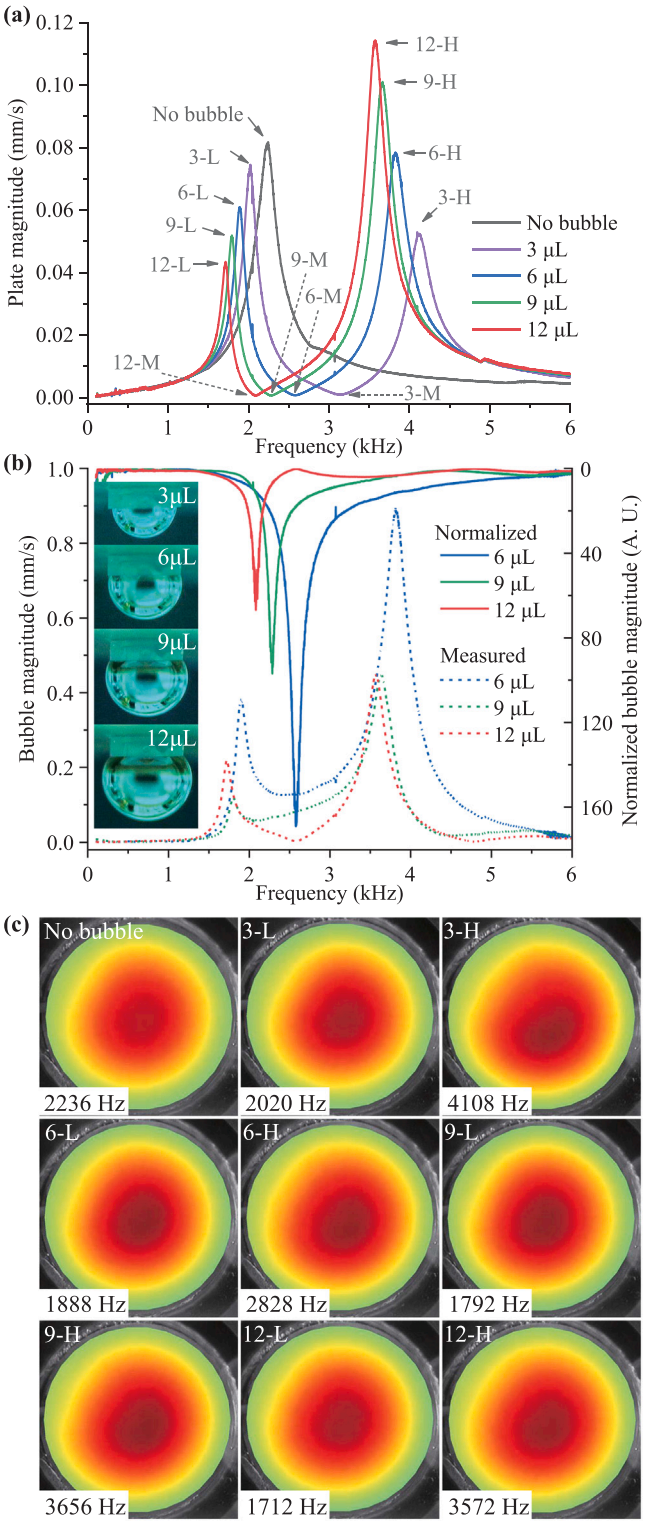

Fig. 2. (a) Frequency response measured at the center point of the piezoelectric plate's upper surface. (b) Frequency response measured at the surface of the air bubble (dashed line) and normalized frequency response of the vibrating bubble (solid line). Inserts are the optical images of different volumes of bubbles. (c) 2D mode shape obtained by the laser vibrometer. Each figure corresponds to a marked peak in (a). The driving amplitude is 0.01 V in all the measurements. Letters L, M and H correspond to the lower peak, middle valley and higher peak observed in (a), respectively.

the peak frequencies in Fig. 2(c) that both peaks of a single curve belong to the same vibration mode (the (0, 1) mode). To further reveal the mechanism of this phenomenon, the frequency response of the air bubble is directly measured with a 45-degree tilted mirror (see Fig. 1 (b)). The absence of a corresponding dashed line in Fig. 2(b) indicates that a bubble of 3 μL volume cannot be detected since its small size failed to generate a tangent point for laser focus. The normalized frequency response of the air bubble is calculated by dividing the frequency response of the bubble by the frequency response of the plate, as shown on the solid lines in Fig. 2(b). Three clear resonance peaks can be observed. They correspond to the intrinsic frequency responses of different sizes of bubbles. A comparison of Fig. 2(a) and (b) shows that the resonance frequency of the bubble is the same as the frequency of the deep valley (the lowest point of the valley, labeled by the dashed arrows in Fig. 2(a)). Considering the vibrating plate and the bubble as two coupled vibration modes, such phenomenon can be explained as an internal resonance between plate and bubble [27]. The deep valley is induced by energy transfer from the piezo plate to the air bubble. The transfer efficiency can reach its maximum value at the resonance frequency of the bubble, leading to a minimum value infrequency response of the plate. By coupling an air bubble to a flexible piezo plate through a bubble trapper, the resonance frequency of the bubble can be obtained by checking the frequency response of the piezoelectric plate. This is much more convenient and simpler than the more difficult and challenging method of using laser Doppler vibrometry or particle image velocimetry to measure bubble vibration. There are other low-cost methods for frequency response measurement of a piezoelectric transducer, such as impedance measurement [28].

Next, when we use the vibrating bubble to generate streaming flows, large vibrational amplitudes in the surface mode of a bubble are required for effective streaming [29]. Three working conditions are considered, according to the dynamic characteristics of the coupled system: vibrating at the frequency of the lower peak, the bottom of the middle valley, and the higher frequency peak (represented by L, M, and H). Optical images of a 9 μL bubble are captured with a high-speed camera using an exposure time of 0.005 ms. The driving voltages for the three conditions are 0.5, 0.6, and 0.4 V, respectively, to maintain a similar vibrating velocity for the L and H conditions, and a relatively higher velocity for the M condition. The images are shown in Fig. 3(a), where the velocities are the values measured at the center point of the piezo plate. All three working conditions can generate surface modes, indicating the possibility of producing streaming flows. Streaming flows are qualitatively characterized by injecting a small amount of methylene blue dye (10 mmol/L in deionized water) near the 9 μL bubble. The driving voltage is kept constant during the image capture experiment. The dye distribution images are shown in Fig. 3(b). For the lower and higher peak conditions, when the plate center has a vibrating velocity of 150 mm/s or more, significant streaming of the flow is observed, but the two streams are in opposite directions. When vibrating at the lower peak frequency, liquid under the bubble is moved upward, then is ejected laterally to form vortices. When the driving frequency is at the higher peak value, the liquid around the bubble is collected, then jetted vertically downward, to generate vortices. If the piezo plate is driven at the bottom of the middle valley frequency (resonance frequency of the bubble), a streaming flow can also be detected, but it is extremely weak. It is most likely caused by the small amplitude of the bubble compared with the amplitudes under the lower peak and higher peak conditions. The red arrows in Fig. 3(b) indicate the direction of the streaming flows, where the solid and dashed lines refer to non-vortical flow and vortical flow, respectively. The dye experiment discussed above is conducted also, by using a vibrating plate and without a bubble. No streaming flow is detected when vibration is initiated. A video of the no-bubble condition, as well as videos of each figure in Fig. 3 are included in the supplemental material. It seems that both lower and higher peak working conditions can transport fresh solution from distant fluid to the vicinity of the air bubble, which is expected to enhance mass transfer. Especially

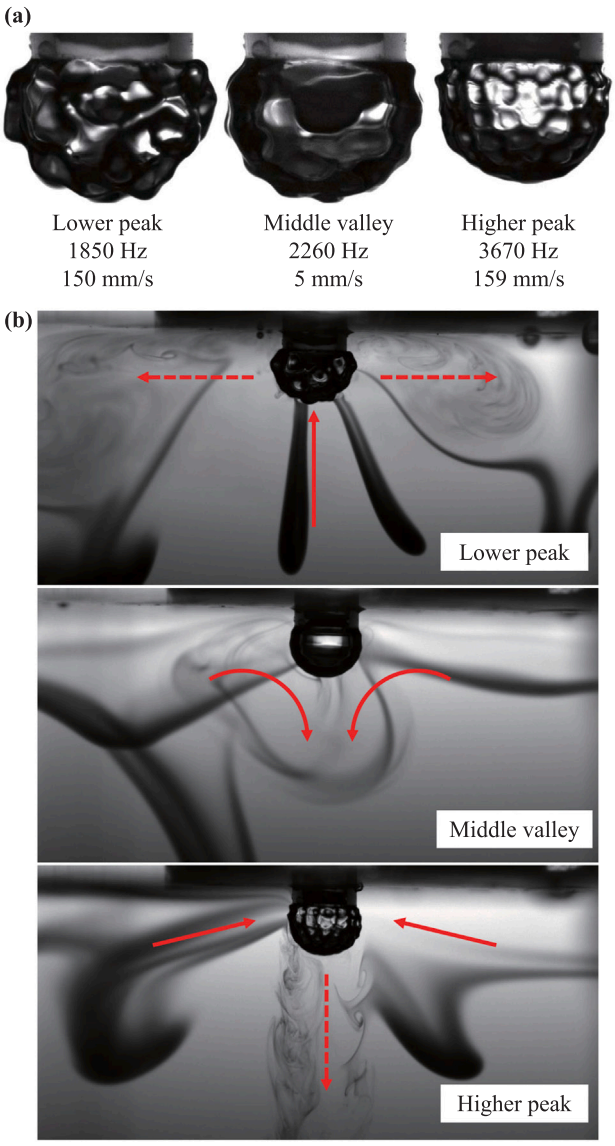

Fig. 3. (a) Optical images of a vibrating bubble at different driving frequencies identified in Fig. 2(a). (b) Streaming flow marked with methylene blue dye near the vibrating bubble. The solid and dashed arrows represent non-vortical flow and flow with vortices, respectively. In all the experiments, the volume of the bubble is 9 μL. Vibrating velocities shown in (a) are measured at the center point of the piezoelectric plate's upper surface. Full videos of the streaming are available in the supplemental material.

for the lower peak condition, the streaming flow generates vortices near the plate surface where the gold working electrode is located. In the next section, mass transfer capabilities with different bubble vibrating conditions are tested using electrochemical methods.

3.2. *Electrochemical experiment with a vibrating bubble*

Mass transfer coefficients under the influence of streaming flows induced by the vibrating bubble are measured with the chronoamperometry method using 2 mmol/L $K_4[Fe(CN)_6]$ as the oxidizing agent. On the working electrode, $[Fe(CN)_6]^{4-}$ is reduced into $[Fe(CN)_6]^{3-}$ with a working potential of − 0.4 V vs. Ag/AgCl reference electrode. The current, induced by the reduction reaction, is used to characterize the mass transfer coefficient since the process is a mass transfer dominant reaction. A 90-second test is applied in each measurement during which the current almost reaches steady state. The

current (proportional to the reaction rate) plotted as a function of time for different bubble working conditions is shown in Fig. 4(a). The lower peak, middle valley, and higher peak for the 9 μL bubble, as well as the condition without a bubble, are measured for various vibrating velocities of the plate. All the working conditions show an increasing trend in current with vibrating velocity, even without a bubble, since vibration of the circular membrane itself generates flow motion and enhances mass transfer [30]. Note that for different bubble vibrating conditions, the steady state current shows a different fluctuation range. The current for each condition of the largest velocities range is within the 0.03 mA range on the Y-axis, shown separately in Fig. S2 of the supplement. For no bubble and middle valley conditions, the current fluctuation is almost as small as that of the static case, since no streaming flow and only a tiny non-vortical flow are observed in these two cases. An increased current fluctuation and large current values are found under the higher-peak conditions. An even higher current value, but a huge current fluctuation, is obtained when the lower peak is used. These two results correspond to the two streaming flow directions in Fig. 3(b). There exists a strong non-vortical flow near the substrate when using the higher peak condition, and a complex pattern of vortices covers the surface of the substrate, when under the lower-peak condition. We calculated the average current in the last five seconds of the test at which a steady state current is reached and plotted it as a function of vibrating velocity of the piezo plate, as shown in Fig. 4(b). The vibrating velocity is selected as a reference quantity since the mass transfer is directly related to the velocity [31]. Although the middle valley condition (vibrating at the resonance frequency of the air bubble) can produce over five times the mass transfer enhancement at a very small plate actuation velocity, such a working frequency is not a good choice if a large mass transfer coefficient is expected. The dynamic characteristics of the coupled system limit the actual amplitude of the bubble to a small value. Operation at the lower and higher peaks are two operational options. The mass transfer coefficients are enlarged 12 and 10 times, respectively, according to the currents measured. The lower peak condition, with a higher mass transfer rate and fluctuation, can be used in electrochemical sensing methods that require only an accumulation of analytes, such as anodic stripping voltammetry (ASV) [32] or adsorptive stripping voltammetry (AdSV) [33]. The higher peak condition, with lower mass transfer rate (still has at least one order of magnitude enhancement) but a smaller fluctuation, can be employed with sensing techniques that need real-time measurement, such as chronoamperometry [34]. In addition, we measured the reduction current with different volumes of bubbles (3, 6, and 12 μL) using the lower peak as the working frequency. Directly measured results are shown in Fig. S3 of the supplement. The steady-state current as a function of plate vibrating velocity is shown in Fig. 4(c). The larger bubbles give higher mass transfer coefficients with plate vibration velocities of the same level. However, a larger bubble more easily becomes unstable under a strong driving force. Occasionally the bubble, or a part of a bubble will escape from the trapper. This led to fewer successful experiments and fewer results for the 12 μL bubble test. Besides, as a coupled system, resonance characteristics of the bubble actuator, which is a piezoelectric plate in this work, must also be considered if optimized performance is expected. This is because the frequencies and amplitudes when operating at the lower and higher peak conditions are determined by both the piezoelectric plate and the bubble dynamics.

Finally, to evaluate the potential application of vibrating bubbles in electrochemical sensors, anodic stripping voltammetry (ASV) is used to detect bismuth ions in a solution (20 ppb Bi^{3+} in 0.1 mol/L HCl). Stripping voltammetric analysis is a well-established electrochemical technique frequently used in metal ion concentration measurement. The significant advantages of such a method include easy operation, low cost, and high sensitivity [35]. In ASV analysis, the peak current height or peak area of the anodic wave is used to quantify the amount of analyte in the solution, which depends on the accumulation of reduced metal [36]. A 9 μL bubble is attached and the piezo plate is driven at the lower

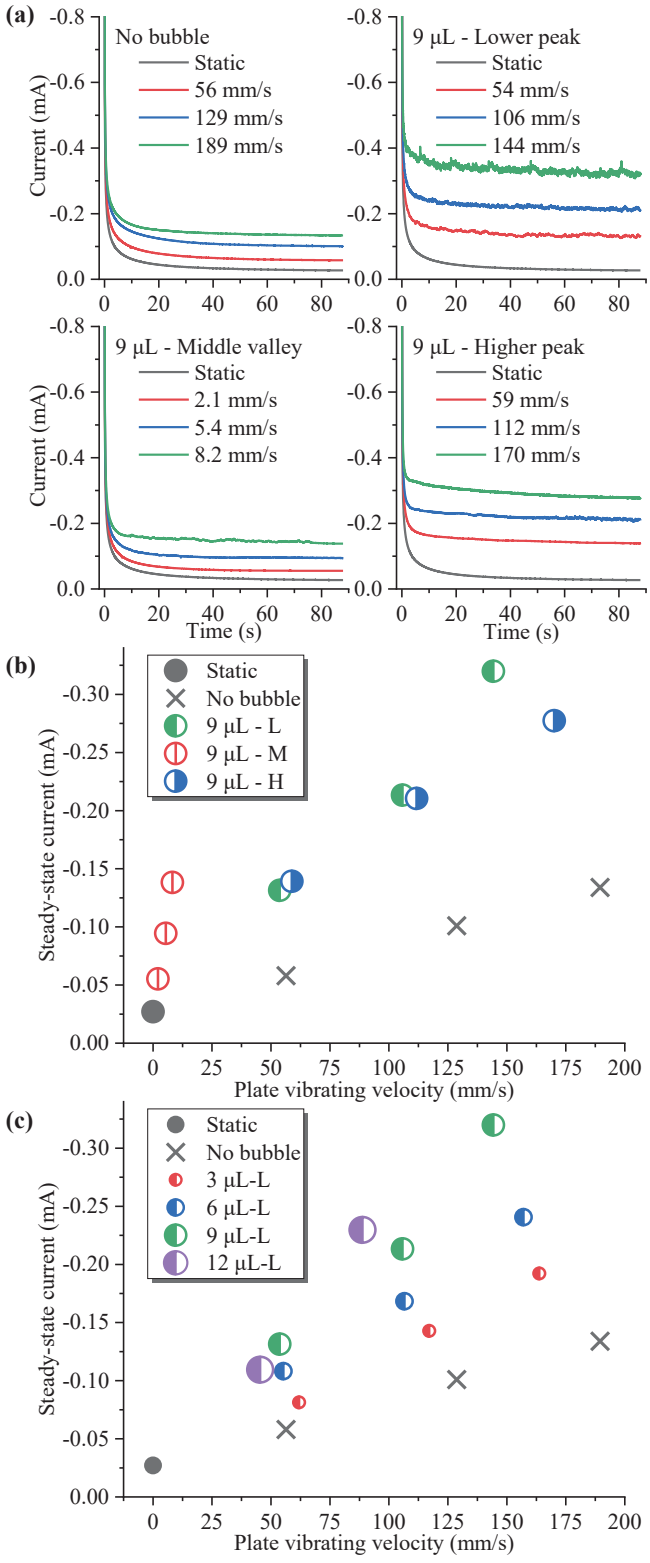

Fig. 4. (a) Chronoamperometry measurement results of the working electrode without bubble (upper left) and with bubble (a 9 μL bubble vibrating at different driving frequencies). (b) and (c) are measured steady-state current as a function of vibrating velocity of the piezoelectric plate. Results for a 9 μL bubble at different driving frequencies are shown in (b), and for different volumes of bubbles at the lower peak frequency are shown in (c). Above experiment is operated in 2 mmol/L $K_4[Fe(CN)_6]$/0.5 mol/L KCl with an electrochemical working potential of − 0.4 V vs. Ag/AgCl.

peak frequency with a velocity of about 100 mm/s. The vibration is activated only during the metal deposition process. The stripping curves are obtained by subtracting the background scan from the analytical scan. The results with and without bubble vibration are shown in Fig. 5 (a). As the deposition time increases from 30 s to 150 s, the height of the stripping peak gradually increases because more bismuth is oxidized during the stripping process. Meanwhile, the stripping peaks under vibrating conditions are much larger than the peaks in the static condition. This is due to the different mass transfer coefficients in the metal deposition process. The stripping peak height is calculated and plotted as a function of deposition time in Fig. 5(b). The bars indicating variability are obtained using four independent measurements. The bars for the vibrating conditions are larger than those for the static case, mostly attributed to vibrating amplitude drift within the series of repeated measurements. The frequency response of the coupled system shows some shift, especially after a long period of vibration. In addition, the stripping peak under the vibrating condition shows a slightly nonlinear increase with deposition time. Such a phenomenon may be explained by the increase in working electrode roughness (increase in surface area) resulting from solid metal deposition [37]. Considering a relatively linear range within deposition time from 30 to 120 s, linear fit curves are plotted in Fig. 5(b). R-Squared correlation values for static and vibrating conditions are 0.995 and 0.992, respectively. The peak current and deposition time can be considered as an approximately linear relationship in this range, in which the slope represents the sensor output increment (peak current) induced by a unit of deposition time. The slope for the static and vibrating conditions are 0.018 and 0.135 μA per second, respectively, demonstrating that the vibrating bubble stirrer accelerates the detection speed of the sensor by over 7 times. These data show that the mass transfer coefficient can be greatly enhanced by streaming flows produced by a vibrating bubble, as the detection speed of the sensor is boosted.

4. Conclusion

In this paper, a vibrating air bubble as a stirrer for an electrochemical sensor is presented. The vibrating system contains a flexible piezoelectric plate coupled to a trapped air bubble, both residing in the liquid environment. A gold working electrode for electrochemical sensing is integrated within the system. The resonance frequency and optimal streaming flow generating frequencies of the air bubble are determined based on the mechanical coupling between the piezo plate and the bubble. Streaming flows generated by the vibrating air bubble are employed to enhance mass transfer efficiency of the integrated working electrode.

From the optical measurement of the vibrational properties of the coupled system, it is found that energy is transferred from the piezo plate to the air bubble, leading to an M-shaped frequency response of the plate. The M-shaped velocity vs. frequency curve contains two peaks and one valley, corresponding to two potential working frequencies for streaming generation, and the resonance frequency of an air bubble. According to the dye tracing experiment, the streaming flows at the two optimal working frequencies (lower peak and higher peak frequencies) are in opposite directions. They can be utilized to study enhancement of mass transfer coefficients on the working electrode. Electrochemical tests indicate that the mass transfer rate increases as the vibration intensity of the piezo plate increases, improving by an order of magnitude compared to the static condition. The results obtained by anodic stripping voltammetry to detect bismuth ions also indicate that, with the help of a vibrating bubble, the sensing performance is significantly improved. We believe that such a design of a piezoelectric-actuated air bubble stirrer with an integrated working electrode can be very promising in electrochemical detection when higher mass transfer rates are required.

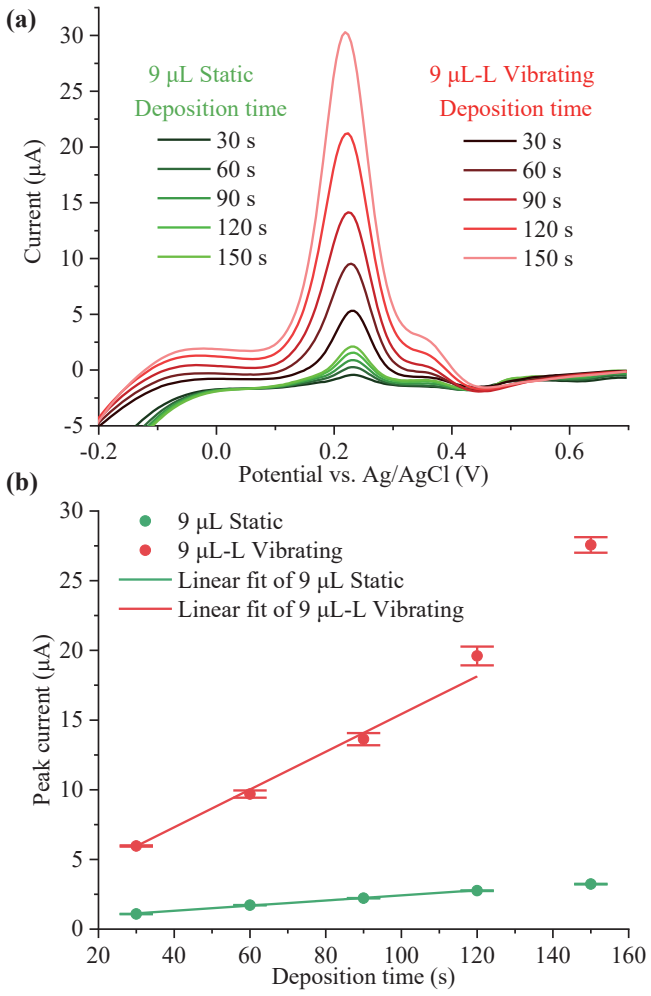

Fig. 5. (a) Anodic stripping voltammetry measurement results for the working electrode in the detection of Bi^{3+} with (red) and without (green) bubble vibration. The 9 μL bubble is driven at the lower peak frequency. (b) Measured stripping peaks as a function of deposition time under static and vibrating conditions (the range for linear fit is from 30 to 120 s). Error bars are calculated with four independent measurement results. The analyte solution contains 20 ppb Bi^{3+} and 0.1 mol/L HCl. The deposition potential is − 0.3 V vs. Ag/AgCl. The letter L represents the lower resonance peak of the piezo plate.

CRediT authorship contribution statement

Tianyi Zhang: Conceptualization, Methodology, Validation, Writing – original draft. **Peng Zhou**: Methodology, Validation. **Terrence Simon**: Methodology, Writing – review & editing. **Tianhong Cui**: Resources, Writing – review & editing, Supervision, Project administration.

Declaration of Competing Interest

The authors declare that they have no known competing financial interests or personal relationships that could have appeared to influence the work reported in this paper.

Acknowledgements

Portions of this work were conducted in the Minnesota Nano Center, which is supported by the National Science Foundation through the National Nano Coordinated Infrastructure Network (NNCI) under Award Number ECCS-2025124. This work was partially sponsored by Environment and Natural Resources Trust Fund (ENRTF) funding

through Legislative-Citizen Commission on Minnesota Resources (LCCMR) in Minnesota State.

Appendix A. Supporting information

Supplementary data associated with this article can be found in the online version at doi:10.1016/j.snb.2021.131218.

References

[1] J. Holmes, P. Pathirathna, P. Hashemi, Novel frontiers in voltammetric trace metal analysis: towards real time, on-site, in situ measurements, Trac Trends Anal. Chem. 111 (2019) 206–219, https://doi.org/10.1016/j.trac.2018.11.003.

[2] M.K. Masud, M. Umer, M.S.A. Hossain, Y. Yamauchi, N. Nam-Trung, M.J. A. Shiddiky, Nanoarchitecture frameworks for electrochemical miRNA detection, Trends Biochem. Sci. 44 (2019) 433–452, https://doi.org/10.1016/j.tibs.2018.11.012.

[3] A. Nsabimana, S.A. Kitte, T.H. Fereja, M.I. Halawa, W. Zhang, G. Xu, Recent developments in stripping analysis of trace metals, Curr. Opin. Electrochem. 17 (2019) 65–71, https://doi.org/10.1016/j.coelec.2019.04.012.

[4] E.E. Ferapontova, DNA electrochemistry and electrochemical sensors for nucleic acids, in: P.W. Bohn, J.E. Pemberton (Eds.), Annual Review of Analytical Chemistry, vol. 112018, pp. 197–218.

[5] E.V. Suprun, V.V. Shumyantseva, A.I. Archakov, Protein electrochemistry: application in medicine. A review, Electrochim. Acta 140 (2014) 72–82, https://doi.org/10.1016/j.electacta.2014.03.089.

[6] A.J. Bard, L.R.J.S.T. Faulkner, Electrochemical Methods Fundamentals and Applications, 20 (1983) 91–92.

[7] T. Kangkamano, A. Numnuam, W. Limbut, P. Kanatharana, T. Vilaivan, P. Thavarungkul, Pyrrolidinyl PNA polypyrrole/silver nanofoam electrode as a novel label free electrochemical miRNA-21 biosensor, Biosens. Bioelectron. 102 (2018) 217–225, https://doi.org/10.1016/j.bios.2017.11.024.

[8] C.S. Chapman, C.M.G. van den Berg, Anodic stripping voltammetry using a vibrating electrode, Electroanalysis 19 (2007) 1347–1355, https://doi.org/10.1002/elan.200703873.

[9] J. Jalal, T.S.H. Leong, Microstreaming and its role in applications: a mini-review, Fluids 3 (2018) 93, https://doi.org/10.3390/fluids3040093.

[10] Y. Gao, M. Wu, Y. Lin, J. Xu, Trapping and control of bubbles in various microfluidic applications, Lab a Chip 20 (2020) 4512–4527, https://doi.org/10.1039/d0lc00906g.

[11] S. Cleve, Microstreaming induced in the vicinity of an acoustically excited, nonspherically oscillating microbubble: Université de Lyon, 2019.

[12] Y. Gao, M. Wu, Y. Lin, W. Zhao, J. Xu, Acoustic bubble-based bidirectional micropump, Microfluid. Nanofluidics 24 (2020) 29, https://doi.org/10.1007/s10404-020-02334-6.

[13] D. Ahmed, C.Y. Chan, S.C. Lin, H.S. Muddana, N. Nama, S.J. Benkovic, T.J. Huang, Tunable, pulsatile chemical gradient generation via acoustically driven oscillating bubbles, Lab a Chip 13 (2013) 328–331, https://doi.org/10.1039/c2lc40923b.

[14] R.H. Liu, R. Lenigk, R.L. Druyor-Sanchez, J.N. Yang, P. Grodzinski, Hybridization enhancement using cavitation microstreaming, Anal. Chem. 75 (2003) 1911–1917, https://doi.org/10.1021/ac026267t.

[15] F.-W. Liu, Y. Zhan, S.K. Cho, Propulsion reversal in oscillating-bubble powered micro swimmer, J. Micromech. Microeng. 31 (2021), 084001, https://doi.org/10.1088/1361-6439/ac0e7f.

[16] D. Ahmed, A. Ozcelik, N. Bojanala, N. Nama, A. Upadhyay, Y. Chen, W. Hanna-Rose, T.J. Huang, Rotational manipulation of single cells and organisms using acoustic waves, Nat. Commun. 7 (2016) 11085, https://doi.org/10.1038/ncomms11085.

[17] A. Hashmi, G. Yu, M. Reilly-Collette, G. Heiman, J. Xu, Oscillating bubbles: a versatile tool for lab on a chip applications, Lab a Chip 12 (2012) 4216–4227, https://doi.org/10.1039/c2lc40424a.

[18] S. An, R. Ranaweera, L. Luo, Harnessing bubble behaviors for developing new analytical strategies, Analyst 145 (2020) 7782–7795, https://doi.org/10.1039/d0an01497d.

[19] Y. Li, X. Liu, Q. Huang, A.T. Ohta, T. Arai, Bubbles in microfluidics: an all-purpose tool for micromanipulation, Lab a Chip 21 (2021) 1016–1035, https://doi.org/10.1039/d0lc01173h.

[20] M.R. Rasouli, M. Tabrizian, An ultra-rapid acoustic micromixer for synthesis of organic nanoparticles, Lab a Chip 19 (2019) 3316–3325, https://doi.org/10.1039/c9lc00637k.

[21] A.J. Conde, I. Keraite, A.E. Ongaro, M. Kersaudy-Kerhoas, Versatile hybrid acoustic micromixer with demonstration of circulating cell-free DNA extraction from sub-ml plasma samples, Lab a Chip 20 (2020) 741–748, https://doi.org/10.1039/c9lc01130g.

[22] T. Yoshikawa, H. Kotera, K. Yoshida, D. Koyama, K. Nakamura, Y. Watanabe, Measurement of the resonant characteristics of a single bubble vibration by using a laser doppler vibrometer, Jpn. J. Appl. Phys. 50 (2011) 07HE04, https://doi.org/10.1143/jjap.50.07he04.

[23] T.F. Argo, P.S. Wilson, V. Palan, Measurement of the resonance frequency of single bubbles using a laser Doppler vibrometer, J. Acoust. Soc. Am. 123 (2008) EL121–EL125, https://doi.org/10.1121/1.2908195.

[24] S. Morioka, M. Ueda, K. Yoshida, D. Koyama, K. Nakamura, Y. Watanabe, Sound pressure threshold of non-spherical oscillation of an attached bubble evaluated by a laser Doppler vibrometer, in: 2012 Ieee International Ultrasonics Symposium 2012, pp. 767–770.

[25] J. Jeon, J. Hong, S.J. Lee, S.K. Chung, Acoustically excited oscillating bubble on a flexible structure and its energy-harvesting capability, Int. J. Precis. Eng. Manuf. Green Technol. 6 (2019) 531–537, https://doi.org/10.1007/s40684-019-00057-w.

[26] M. Guedra, C. Inserra, C. Mauger, B. Gilles, Experimental evidence of nonlinear mode coupling between spherical and nonspherical oscillations of microbubbles, Phys. Rev. E 94 (2016), 053115, https://doi.org/10.1103/PhysRevE.94.053115.

[27] T. Zhang, C. Guo, Z. Jiang, X. Wei, Internal resonance between the extensional and flexural modes in micromechanical resonators, J. Appl. Phys. 126 (2019) 537–540, https://doi.org/10.1063/1.5115028.

[28] G. Tang, B. Yang, C. Hou, G. Li, J. Liu, X. Chen, C. Yang, A piezoelectric micro generator worked at low frequency and high acceleration based on PZT and phosphor bronze bonding, Sci. Rep. 6 (2016) 38798, https://doi.org/10.1038/srep38798.

[29] C. Wang, B. Rallabandi, S. Hilgenfeldt, Frequency dependence and frequency control of microbubble streaming flows, Phys. Fluids 25 (2013), 022002, https://doi.org/10.1063/1.4790803.

[30] T. Zhang, P. Zhou, T. Simon, T. Cui, Ieee, A circular vibrating electrode with enhanced mass transfer for high-performance electrochemical sensors, in: 2021 34th Ieee International Conference on Micro Electro Mechanical Systems 2021, pp. 779–782.

[31] M.H. Abdel-Aziz, I. Nirdosh, G.H. Sedahmed, Mass and heat transfer behavior of oscillating helical coils in relation to heterogeneous reactor design, Aiche J. 63 (2017) 3141–3149, https://doi.org/10.1002/aic.15614.

[32] G. Batley, T.J.J.o.E.C. Florence, I. Electrochemistry, An evaluation and comparison of some techniques of anodic stripping voltammetry, 55 (1974) 23–43,

[33] M.G. Paneli, A. Voulgaropoulos, Applications of adsorptive stripping voltammetry in the determination of trace and ultratrace metals, Electroanalysis 5 (1993) 355–373, https://doi.org/10.1002/elan.1140050502.

[34] D. Grieshaber, R. MacKenzie, J. Vörös, E.J.S. Reimhult, Electrochemical biosensors-sensor principles and architectures, 8 (2008) 1400–1458.

[35] Y. Lu, X. Liang, C. Niyungeko, J. Zhou, J. Xu, G. Tian, A review of the identification and detection of heavy metal ions in the environment by voltammetry, Talanta 178 (2018) 324–338, https://doi.org/10.1016/j.talanta.2017.08.033.

[36] T. Zhang, Q. Liu, X. Wei, Z. Jiang, T. Cui, A vibrating membrane working electrode for highly sensitive anodic stripping voltammetry, Sens. Actuators B Chem. 311 (2020), 127948, https://doi.org/10.1016/j.snb.2020.127948.

[37] R. Venkatasubramanian, K. Jin, N.S. Pesika, Use of electrochemical deposition to create randomly rough surfaces and roughness gradients, Langmuir 27 (2011) 3261–3265, https://doi.org/10.1021/la200245m.

Tianyi Zhang was born in Qinhuangdao, Hebei, China in 1990. He received his B.S. and Ph.D. degrees from the Department of Mechanical Engineering at Xi'an Jiaotong University (Xi'an, Shanxi, China) in 2013 and 2019. He spent one year at the University of Minnesota as a visiting scholar. He is now a post-doctoral associate of the Department of Mechanical Engineering at the University of Minnesota. His research interests include vibration mode coupling in micromechanical resonators & oscillators and mass transport in electrochemical sensing applications.

Peng Zhou was born in Ningguo, Anhui, China in 1993. He received the B.S. in 2015 from the Department of Mechanical Engineering at Beijing Institute of Technology, China. Then he got M.S. degrees in mechanical engineering from the Purdue University Northwest, USA. He is currently a Ph.D. candidate student guided by Prof. Tianhong Cui in the Department of Mechanical Engineering in the University of Minnesota. His research interests include the photocatalytic water purification and MEMS based microsensors for both environmental and biomedical applications.

Terrence W. Simon received the B.S. degree in mechanical engineering from Washington State University, Pullman, WA, in 1968 and the M.S. degree in mechanical engineering from the University of California at Berkeley, Berkeley, CA, in 1971. He received the Ph.D. degree in mechanical engineering from Stanford University, Stanford, CA, in 1980. He is the Ernst G. Eckert Professor of the Department of Mechanical. His major research interests include experiments, computation and visualization of heat, mass and momentum transfer in laminar, turbulent, transitional and unsteady flows, including flows through porous media and processes with phase change. Applications range from flow and heat transfer in plasma cutting tools and plasma flow actuators, electronics and optics, Stirling and gas turbine engines, and MW-level grid energy storage systems. Dr. Simon is an active member of the American Society of Mechanical Engineers (including a past five-year term as the Senior Technical Editor of the Journal of Heat Transfer), the International Centre for Heat and Mass Transfer (in which he is now the President and has served on the Executive Committee), and the American Society of Thermal and Fluids Engineers (for which he co-chaired the International Workshop on Heat Transfer in 2017).

Tianhong Cui (SM'04) received the B.S. degree in mechanical engineering from Nanjing University of Aeronautics and Astronautics, Nanjing, Jiangsu, China, in 1991 and the Ph.D. degree in mechanical engineering from the Chinese Academy of Sciences, Changchun, Jilin, China, in 1995. He is currently a Distinguished McKnight University Professor at the University of Minnesota. From 1995–2003, he held research or faculty positions at Tsinghua University, University of Minnesota, National Laboratory of Metrology in Japan, and Louisiana Tech University. His current research interests include MEMS and nanotechnology. Dr. Cui is an Adjunct Professor at Mayo Clinic, a Distinguished Visiting Fellow at the University of Cambridge, and a Distinguished Visiting Professor at University of Paris-Est in France. He is a Fellow of American Society of Mechanical Engineering (ASME). He is the founding Executive Editor-in-Chief for two Nature journals, *Light: Science & Applications* and *Microsystems & Nanoengineering*. He is also serving as the founding Editor-in-Chief for the first AAAS/Science Partner Journal titled *Research*.